Enhancing field emission from a carbon nanotube array by lateral control of electrodynamic force field

D. Roy Mahapatra [a]; S. V. Anand [a]; N. Sinha [b]; R. V. N. Melnik [c]

[a] Department of Aerospace Engineering, Indian Institute of Science, Bangalore, India [b] Department of Mechanical Engineering, Massachusetts Institute of Technology, Cambridge, MA, USA [c] M²NeT Lab, Wilfrid Laurier University, Waterloo, ON, Canada

PLEASE SCROLL DOWN FOR ARTICLE

Enhancing field emission from a carbon nanotube array by lateral control of electrodynamic force field

D. Roy Mahapatra[a]*, S.V. Anand[a], N. Sinha[b] and R.V.N. Melnik[c]

[a]*Department of Aerospace Engineering, Indian Institute of Science, Bangalore 560012, India; [b]Department of Mechanical Engineering, Massachusetts Institute of Technology, Cambridge, MA 02139-4307, USA; [c]M²NeT Lab, Wilfrid Laurier University, Waterloo, ON, Canada, N2L 3C5*

Fluctuation of field emission current from carbon nanotubes (CNTs) poses certain difficulties for their use in nano-biomedical X-ray devices and imaging probes. This problem arises due to deformation of the CNTs due to electrodynamic force field and electron–phonon interaction. It is of great importance to have precise control of emitted electron beams very near the CNT tips. In this paper, a new array configuration with stacked array of CNTs is analysed and it is shown that the current density distribution is greatly localised at the middle of the array, that the scatter due to electrodynamic force field is minimised and that the temperature transients are much smaller compared to those in an array with random height distribution.

Keywords: carbon nanotube arrays; field emission; coupled effects; biomedical X-ray imaging; cancer treatment; transport phenomena

1. Introduction

Field emission from carbon nanotubes (CNTs) was first reported in 1995 by three research groups [1–3]. With significant research attention, CNTs are currently ranked among the best field emitters. CNTs grown on substrates are used as electron sources in field emission applications. Several studies have reported the use of CNTs in field emission devices, including field emission displays, X-ray tube sources, electron microscopes, cathode-ray lamps, etc. [4–7]. Also, in recent years, conventional cold field emission cathodes have been realised in micro-fabricated arrays for medical X-ray imaging [8] and today CNT-based field emission cathode devices can readily produce both continuous and pulsed X-ray for a variety of industrial and medical applications [9], including recent applications for cancer treatment [10]. Field emission performance of a single isolated CNT is found to be remarkable, but the situation becomes complex when an array of CNTs is used [11]. At the same time, use of arrays of CNTs is known to be practical and economical. Indeed, such arrays on cathode substrates can be grown easily and their collective dynamics can be utilised in a statistical sense such that the average emission intensity is high enough and the collective dynamics lead to longer emission life. The modelling process of CNT arrays and associated devices requires the development of multiphysics approaches due to a range of coupled processes and transport phenomena involved [12,13].

This development has been discussed in detail in recent papers [14–17]. In particular, in [14] field emission properties of open and closed single-walled CNTs were analysed. In [15], for the first time, a systematic multiphysics based modelling approach was proposed to analyse the evolution and self-assembly of randomly oriented CNTs and the results of this analysis were applied to thin-film emitting diodes. Electromechanical effects in such devices were studied in detail in [16] as these effects are known to be able to augment significantly the properties of nanostructures [18]. More recently, in [17] a systematically coupled model accounting for both the electron–phonon transport and the mechanical deformation in the CNTs has been proposed. Based on earlier analyses, we have concluded that field emission from CNTs is difficult to characterise using simple formulae or data fitting due to several physical phenomena involved: (1) electron–phonon interaction; (2) electromechanical force field leading to deformation of CNTs; and (3) ballistic transport induced thermal spikes, coupled with high dynamic stress, leading to degradation of emission performance. Recently, a number of advances have been made along these lines. Indeed, fairly detailed physics-based models of CNTs considering the aspects (1) and (2) above have already been developed by the authors [17,19,20]. For a matrix of CNTs, an analytical estimate of field enhancement factor including the effect of Coulomb field, image potential and anode–cathode

---

*Corresponding author. Email: droymahapatra@aero.iisc.ernet.in

distance was reported by Wang et al. [21]. Effects of vertical alignment of CNTs and substrates on the field emission current–voltage characteristics were studied experimentally by Chen et al. [22]. Effect of spacing and diameter of CNTs in the arrays have been studied in [23]. Advances in patterning of CNTs for field emission applications have also been recently made (see e.g. [24]).

In [15], the present authors developed a model of interacting CNTs including the effect of random CNTs on cathode substrate (termed as CNT based thin film). The I–V curves obtained from this model were compared with experimental results and found to be in good agreement. Subsequently, the transient phenomena and statistics of the CNT arrays were analysed both experimentally and based on a refined version of the previous model of CNT array in [16,17]. With reference to this model, one would be able to realise how the present idea of pointed array of CNTs has been developed. However, design optimisation issues aimed at better field emission devices to reduce the extent of electro-mechanical fatigues and to improve spatio-temporal localisation of emitted electrons remain open and are important areas of research. With due success in designing such devices, various applications such as *in situ* biomedical X-ray probes and thin film pixel based imaging technology, to name just a few, are of great significance. The authors' interest in this study stems from the problem of precision biomedical X-ray generation. In this paper, we focus on the device-level performance of CNTs grown on a metallic surface in the form of an array (for field emission) under diode configuration. We analyse a new design concept, wherein (a) the electrodynamic force field leading to strong electron–phonon interaction during ballistic transport and also (b) the usually observed reorientation of the CNT tips and instability due to Coulomb repulsions can be harnessed optimally.

2. Model formulation

We first discuss the basic modelling framework in this section and then formulate the model of electrodynamic force field by considering individual CNTs in the array as one-dimensional elements for transport of electron–gas with appropriate boundary conditions.

Let N_T be the total number of carbon atoms including those in CNTs and those in cluster forms as a mesoscopic description of the surface of the cathode substrate and in a representative volume element $V_{cell} = \Delta A d$. Here, ΔA is the computational cell surface interfacing the anode and d is the distance between the inner surfaces of cathode substrate and the anode. Let N be the number of CNTs in the cell, and N_{CNT} be the total number of carbon atoms present in the CNTs. We assume that during field emission, some of the CNT structures are decomposed and they form clusters. Such degradation and fragmentation of CNTs can

be treated as the reverse process of Chemical Vapour Deposition (CVD) or a similar growth process used for producing the CNTs on a substrate. Hence,

$$N_T = N N_{CNT} + N_{cluster}, \tag{1}$$

where $N_{cluster}$ is the total number of carbon atoms in the clusters in a cell at time t and it is given by

$$N_{cluster} = V_{cell} \int_0^t dn_1(t), \tag{2}$$

where n_1 is the concentration of carbon clusters in the cell. By combining Equations (1) and (2), one has

$$N = \frac{1}{N_{CNT}} \left[N_T - V_{cell} \int_0^t dn_1(t) \right]. \tag{3}$$

The number of carbon atoms in a CNT is proportional to its length. Let the length of a CNT be a function of time, denoted as $L(t)$. Therefore, one can write

$$N_{CNT} = N_{ring} L(t), \tag{4}$$

where N_{ring} is the number of carbon atoms per unit length of a CNT and it can be determined from the geometry of the hexagonal arrangement of carbon atoms in the CNT. By combining Equations (3) and (4), one can write

$$N = \frac{1}{N_{ring} L(t)} \left[N_T - V_{cell} \int_0^t dn_1(t) \right]. \tag{5}$$

In order to determine $n_1(t)$ phenomenologically, we employ a nucleation coupled model developed previously in [19]. Based on the model, the rate of degradation of CNTs (v_{burn}) is defined as

$$v_{burn} = V_{cell} \frac{dn_1(t)}{dt} \left[\frac{s(s-a_1)(s-a_2)(s-a_3)}{n^2 a_1^2 + m^2 a_2^2 + nm(a_1^2 + a_2^2 - a_3^2)} \right]^{1/2}, \tag{6}$$

where a_1, a_2, a_3 are lattice constants, $s = (1/2)(a_1 + a_2 + a_3)$, n and m are integers ($n \geq |m| \geq 0$). The pair (n, m) defines the chirality of the CNT. Therefore, at a given time, the length of a CNT can be expressed as $h(t) = h_0 - v_{burn} t$, where h_0 is the initial average height of the CNTs and d, as before, is the distance between the cathode substrate and the anode.

The surface electron density of CNTs ($\tilde{n}$) can be expressed as the sum of a steady (unstrained) part ($\tilde{n}_0$) and a dynamically strained part ($\tilde{n}_0$). Therefore, $\tilde{n} = \tilde{n}_0 + \tilde{n}_1$, where the steady part $\tilde{n}_0$ is the surface electron density corresponding to the Fermi level energy in the unstrained CNT and it can be approximated as [25] $\tilde{n}_0 = kT/(\pi b^2 \Delta)$, where k is Boltzmann's constant, T is the absolute temperature, b is the interatomic distance and Δ is the

overlap integral ($\approx 2\,\mathrm{eV}$ for carbon). The fluctuating part $\tilde{n}_1$ is inhomogeneous along the length of the CNTs. Actually, $\tilde{n}_1$ should be coupled nonlinearly with the deformation and the electromagnetic field [26]. However, in a simplified form, $\tilde{n}_1$ is primarily governed by one of the quantum-hydrodynamic equations. The deformation of CNTs during field emission is a combined effect of various electromechanical forces in a slow time scale and the fluctuation of the CNT sheet due to electron–phonon interaction in a fast time scale. Therefore, the total displacement u_{total} can be expressed as

$$u_{\mathrm{total}} = u^{(1)} + u^{(2)}, \tag{7}$$

where $u^{(1)}$ and $u^{(2)}$ are the displacements due to electromechanical forces and fluctuations of CNT sheets due to electron–phonon interaction, respectively. The elements of displacement vector in the coordinate system (x', y', z') with z' being the tangent to the curved tube axis, can be written as

$$u^{(1)} = \left\{ u_{x'}^{(1)} u_{z'}^{(1)} \right\}^{\mathrm{T}}, \quad u^{(2)} = \left\{ u_{x'}^{(2)} u_{z'}^{(2)} \right\}^{\mathrm{T}}, \tag{8}$$

where $u_{x'}$ is the lateral displacement and $u_{z'}$ is the longitudinal displacement at a length-wise location of CNTs where the CNT cross-sections are reduced to a point, thus by neglecting the radial breathing modes. Furthermore, to simplify the analysis, we consider only one component of lateral motion and remove the y' dependence of the motion in the slow time scale. In the array, each CNT is treated as a one-dimensional elastic member discretised by fictitious segments and nodes with equivalent electronic charges lumped on the nodes. The electrodynamic force field is computed as discussed in [17].

In the fast time scale, the displacement field $u^{(2)}$ is coupled with the density of state via the changes in the atomic coordinates due to electrodynamic force. The electrodynamic force field comprises of Coulomb force due to pair-wise interaction of CNTs in the array and the electrodynamic force due to conduction electrons within a CNT. The density of state is further influenced by the electromagnetic field and self-interaction potentials. Such a dynamic interaction between the electrons and the electromagnetic field can be expressed as

$$\begin{aligned}
&\frac{\partial^2 \tilde{n}_1}{\partial t^2} - \frac{e\tilde{n}_0}{m_{\mathrm{e}}}\frac{\partial E_{z'}}{\partial z'} - \alpha_2 \frac{\partial^2 \tilde{n}_1}{\partial z'^2} + \beta_2 \frac{\partial^4 \tilde{n}_1}{\partial z'^4} + \frac{\beta_2}{r^2}\frac{\partial^2}{\partial z'^2}\left(\frac{\partial^2 \tilde{n}_1}{\partial \theta_0^2}\right) \\
&\quad + \frac{n_0}{m_{\mathrm{e}}}\frac{\partial f_{lz'}}{\partial z'} - \frac{e\tilde{n}_0}{m_{\mathrm{e}}}\frac{1}{r}\frac{\partial E_{\theta_0}}{\partial \theta_0} - \frac{\alpha_2}{r^2}\frac{\partial^2 \tilde{n}_1}{\partial \theta_0^2} + \frac{\beta_2}{r^4}\frac{\partial^4 \tilde{n}_1}{\partial \theta_0^4} \\
&\quad + \frac{\beta_2}{r^2}\frac{\partial^2}{\partial \theta_0^2}\left(\frac{\partial^2 \tilde{n}_1}{\partial z'^2}\right) + \frac{n_0}{m_{\mathrm{e}}}\frac{1}{r}\frac{\partial f_{l\theta_0}}{\partial \theta_0} - \frac{en_0}{m_{\mathrm{e}}}\frac{\partial E_r}{\partial r} \\
&\quad + \frac{n_0}{m_{\mathrm{e}}}\frac{\partial f_{lr}}{\partial r} + \frac{n_0}{m_{\mathrm{e}}}\frac{\partial f_{pr}}{\partial r} = 0, \tag{9}
\end{aligned}$$

where (r, θ_0, z') defines the cylindrical coordinate system for a CNT with $r = R$ as the CNT radius, m_{e} is the effective mass of electron, α_2 is the speed of propagation of density disturbances, β_2 is the single electron excitation in the electron gas, f_l is the Lorentz force, f_p is the ponderomotive force, and $E_{z'}$, E_{θ_0} and E_r are the axial, circumferential and out-of-plane components of the electric field, respectively. The electric field satisfies the Maxwell's equation for the effective medium:

$$\nabla^2 E - \mu\sigma\frac{\partial E}{\partial t} - \mu\epsilon\frac{\partial^2 E}{\partial t^2} = \mu\frac{\partial J}{\partial t}, \tag{10}$$

where μ, σ, ϵ, and J are the magnetic permeability, electric conductivity, electric permittivity, and electric current density in a CNT as an effective medium, respectively. The current density in the CNT sheet can be approximated as

$$J \approx e\tilde{n}\left(v_0 + \frac{\partial u_{z'}^{(2)}}{\partial t} + c_p\frac{\partial u_{z'}^{(2)}}{\partial z'}\right), \tag{11}$$

where v_0 is the velocity of conduction of electrons in the unstrained CNT, c_p is the phase speed of sound propagation along z' direction. Substituting this in Equation (10) and expanding, we get

$$\begin{aligned}
&\frac{\partial^2 E_{z'}(r)}{\partial z'^2} + \frac{1}{r^2}\frac{\partial^2 E_{z'}(r)}{\partial \theta_0^2} + \frac{1}{r}\frac{\partial}{\partial r}\left(r\frac{\partial E_{z'}(r)}{\partial r}\right) \\
&\quad - \mu\sigma\frac{\partial E_{z'}(r)}{\partial t} - \mu\epsilon\frac{\partial^2 E_{z'}(r)}{\partial t^2} = \mu\frac{\partial}{\partial t}\left(e\tilde{n}\frac{\partial u_z^{(2)}}{\partial t}\right),
\end{aligned} \tag{12}$$

$$\begin{aligned}
&\frac{\partial^2 E_{\theta_0}(r)}{\partial z'^2} + \frac{1}{r^2}\frac{\partial^2 E_{\theta_0}(r)}{\partial \theta_0^2} + \frac{1}{r}\frac{\partial}{\partial r}\left(r\frac{\partial E_{\theta_0}(r)}{\partial r}\right) \\
&\quad - \mu\sigma\frac{\partial E_{\theta_0}(r)}{\partial t} - \mu\epsilon\frac{\partial^2 E_{\theta_0}(r)}{\partial t^2} = 0,
\end{aligned} \tag{13}$$

$$\begin{aligned}
&\frac{\partial^2 E_r(r)}{\partial z'^2} + \frac{1}{r^2}\frac{\partial^2 E_r(r)}{\partial \theta_0^2} + \frac{1}{r}\frac{\partial}{\partial r}\left(r\frac{\partial E_r(r)}{\partial r}\right) \\
&\quad - \mu\sigma\frac{\partial E_r(r)}{\partial t} - \mu\epsilon\frac{\partial^2 E_r(r)}{\partial t^2} = 0.
\end{aligned} \tag{14}$$

In the absence of electronic transport within and field emission from the tip of a CNT, the background electric field is simply $E_0 = -V_0/d$, where $V_0 = V_{\mathrm{d}} - V_{\mathrm{s}}$ is the applied bias voltage, V_{s} is the constant source potential on the substrate side, V_{d} is the drain potential on the anode side and d, as before, is the clearance between the electrodes. The total electrostatic energy consists of a linear drop due to the uniform background electric field and the potential energy due to the charges on the CNTs. Therefore, the total electrostatic energy

can be expressed as

$$\mathscr{V}(x,z) = -eV_s - e(V_d - V_s)\frac{z}{d}$$
$$+ \sum_j G(i,j)(\hat{n}_j - n), \qquad (15)$$

where e is the positive electronic charge, $G(i,j)$ is the Green's function [27] with i indicating the ring position and $\hat{n}_j$ describing the electron density at node position j on the ring. In the present case, while computing the Green's function, we also consider the nodal charges of the neighbouring CNTs. This essentially introduces non-local contributions due to the array of CNTs. We compute the total electric field $E = -\nabla\mathcal{V}/e$, which is expressed as

$$E_z = -\frac{1}{e}\frac{d\mathcal{V}(z)}{dz}. \qquad (16)$$

The current density (J) due to field emission is obtained by using the Fowler–Nordheim equation [28]

$$J = \frac{BE_z^2}{\Phi}\exp\left[-\frac{C\Phi^{3/2}}{E_z}\right], \qquad (17)$$

where Φ is the work function of the CNT, and B and C are constants. Computation is performed at every time step, followed by update of the geometry of the CNTs. As a result, the charge distribution among the CNTs also changes and such a change affects the electrostatic energy according to Equation (15). The field emission current (I_{cell}) from the anode surface corresponding to an elemental volume V_{cell} containing an array of CNTs is then obtained as

$$I_{\text{cell}} = A_{\text{cell}}\sum_{j=1}^N J_j, \qquad (18)$$

where A_{cell} is the anode surface area and N is the number of CNTs in the volume element. The total current is obtained by summing the cell-wise current (I_{cell}). This formulation takes into account the effect of CNT tip orientations, and one can perform statistical analysis of the device current for randomly-distributed and randomly-oriented CNTs.

3. Results and discussion

In the proposed design of CNT array based field emission, we introduce two additional gates on the edges of the cathode substrate. An array of stacked CNTs is considered on the cathode substrate. Figure 1 shows a three-dimensional schematic of the CNT array with electrodes as a single pixel. Due to circular symmetry, we consider a two-dimensional configuration of a line of CNT array in the simulation. The height of the CNTs is such that a symmetric force field is maintained in each pixel with
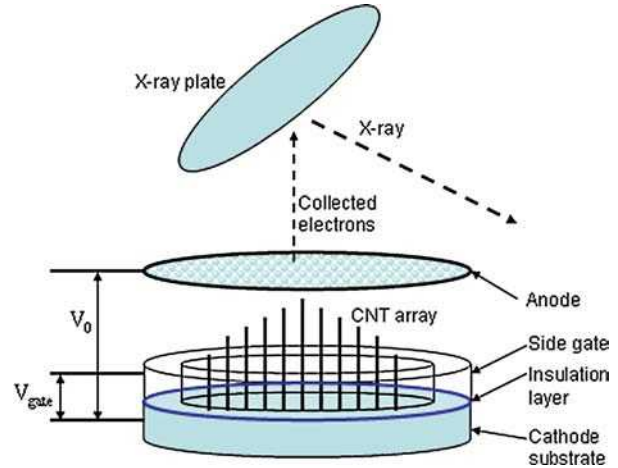

Figure 1. Schematic setup of the CNT array based field emission pixel.

respect to the central axis parallel to z-axis (see Figure 2). As a result, it is expected that a maximum current density and a well-shaped beam can be produced under DC voltage across the cathode and anode. In the present design, the anode is assumed to be simply a uniform conducting slab. However, such an anode can be replaced with a porous thin film along with MEMS-based beam control mechanism. Figure 2 shows the transverse electric field distribution (E_z) in the pixel, which directly influences the field emission.

We consider 100 CNTs in an array for all the simulations. In the simulations, the distance between the cathode substrate and the anode surface was taken as
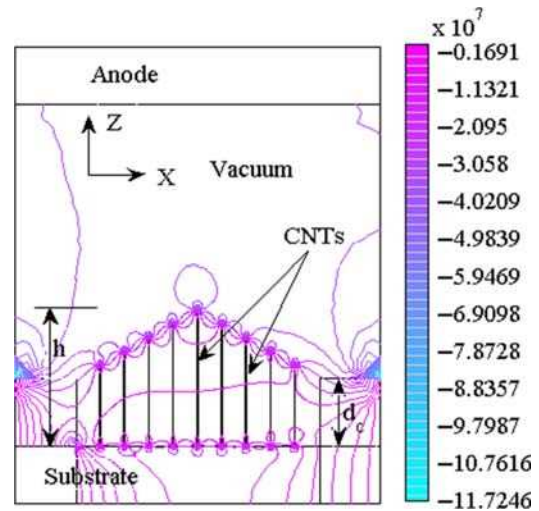

Figure 2. Contour plot showing concentration of electric field E_z surrounding the CNT tips under symmetric lateral force field. $V_0 = 650\,\text{V}$ and the side-wise gates are shorted with the cathode substrate. Electric field contours are shown in V/m unit in the colourbar.

34.7 μm. The height of the side-wise gates was 6 μm, while the spacing between neighbouring CNTs in the array was selected as 2 μm. A DC bias voltage of 650 V is applied across the cathode and anode. We compare the two cases of height distributions of CNTs in the array. In one of these cases, where the CNTs were stacked like a pointed shape, the height was varied from 6 μm at the edges to 12 μm at the centre. In the other case, we chose a random height distribution for the CNTs in the array, where the height was varied as $h = (h_0 \pm 2\,\mu m) \mp 2\,\mu m \times \mathrm{rand}(1)$. Here, the function rand denotes random number generator. The constants B and C in Equation (17) were taken as $(1.4 \times 10^{-6}) \times \exp((9.8929) \times \Phi^{-1/2})$ and 6.5×10^7, respectively [29]. It has been reported in literature (e.g., [29]) that the work function Φ for CNTs is smaller than the work functions for metal, silicon, and graphite. However, there are significant variations in the experimental values of Φ depending on the types of CNTs (i.e. SWNT/MWNT) and geometric parameters. The type of substrate material also has significant influence on the electronic band-edge potential.

The results reported in this paper are based on a representative value of $\Phi = 2.2\,\mathrm{eV}$.

Figure 3(a) shows well stabilised CNTs owing to the electrodynamic interaction due to the pointed shape as compared to the random distribution in Figure 3(b). During 50 s of field emission simulated in these results, the strong influence of lateral force field can be clearly seen. Such force field produces electrodynamic repulsion such that the resultant force imbalance on the CNTs towards the edges of the array eventually destabilises the orientation of the CNT tips. Since, in the pointed shape (see Figure 3(a)), this force imbalance is minimised due to gradual reduction in the CNT heights, a lesser magnitude of deflections is observed. Also, the lateral electrodynamic forces produce instabilities in the randomly distributed array, where the electrons are pulled up by the anode and the CNTs tips experience a significant elongation as shown in Figure 3(b). This is further quantified by the tip angle distribution before and after 50 s of field emission as shown in Figure 4(b) for a random height distribution as compared to Figure 4(a) for the pointed shape. It should
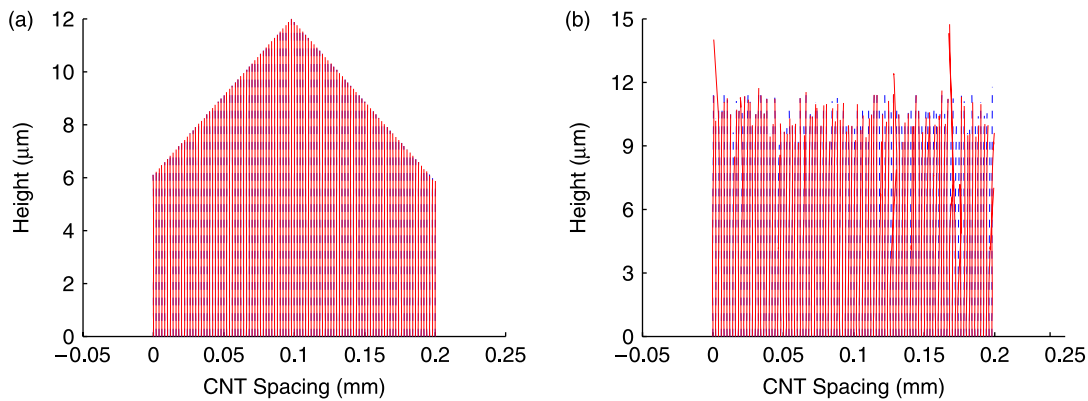

Figure 3.   Visualisation of initial and deflected shape of an array of 100 CNTs at $t = 50$ s of field emission for (a) pointed and (b) random configurations. The dotted lines indicate initial CNTs.
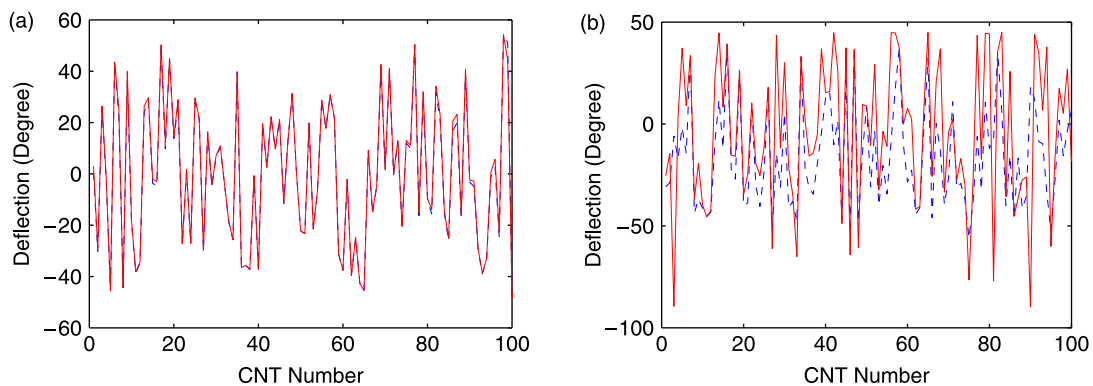

Figure 4.   Tip deflections of each CNT in an array of 100 CNTs at $t = 50$ s of field emission for (a) pointed and (b) random configurations. Dotted line indicates initial tip orientation angle.
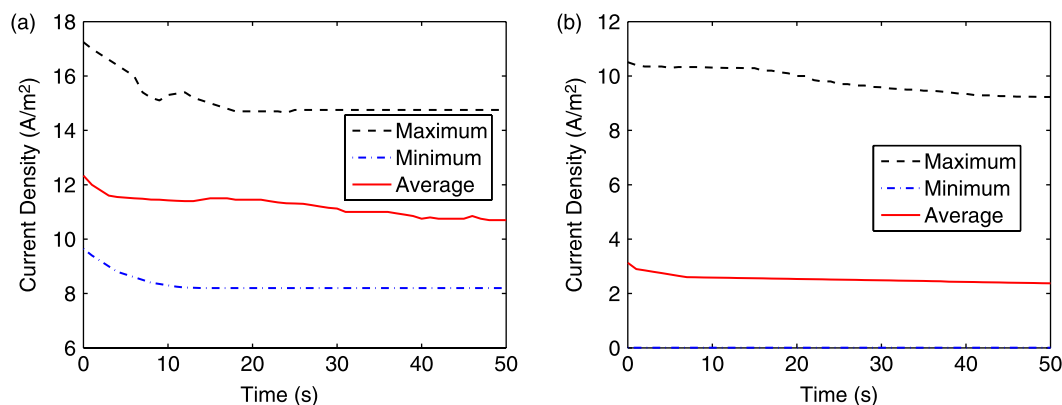
Figure 5. Time history of field emission current density for an array of 100 CNTs at $t = 50$ s of field emission for (a) pointed shape and (b) random height distribution.

be noted that in the simulation, the initial tip deflections are prescribed as a random distribution for both the cases. Due to this reason, the tip orientation angles in Figure 4(a) are also large in the case of pointed shape, but these do not change over time.

In Figure 5(a) and (b) we compare the time histories of maximum, minimum and average current densities out of the array for the case of pointed shape and the case of random height distribution. The average current density for the case of pointed shape is almost three times more than the average current density for the case of random height distribution. This is an interesting result, which clearly demonstrates the improvement achieved by using a pointed shape of the array and the side gate. Also, due to lateral force field induced instabilities in the case of random height distribution, the scatter in the current density distribution in the array is much higher compared to the case of pointed shape. It should also be noted that beside a threefold increase in the magnitude of average current density for the pointed array case in Figure 5(a), the temporal fluctuation is also insignificant as compared to Figure 5(b). This indicates an improved field emission with good stability. Figure 6 shows the spatial distribution of emission current density in the pointed array as compared to the random array. It is clear that the emission is stable and it is focused towards the middle of the array.

Finally, the temperature at the tip of each CNT over an array of 100 CNTs was computed in this study. Note in this context that during the emission of the electrons, interactions among several quantum states and acoustic-thermal phonon modes take place. As the electrons become ballistic electrons in free space, the corresponding energy released to the CNT cap region produces thermal transients. A mesoscopic model of heat generation and transport in CNTs from the tip region [17] is employed in the present computation. Figure 7(a) and (b) shows the temperature at the CNT tips at $t = 50$ s corresponding
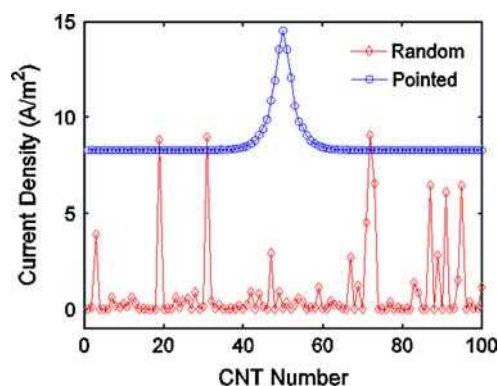

Figure 6. Distribution of current density over the tips of the CNTs in the arrays at $t = 50$ s. The pointed array shows a focused emission.

to Figures 3 and 5 for the cases of pointed shape and random height distribution, respectively. Figure 7(a) shows a temperature rise of up to ≈ 480 K which is at the middle of the array. Another interesting observation is that the temperature distribution profile shows a more or less gradual decrease towards the edges. On the other hand, as seen in Figure 7(b), the random height distribution leads to a much stronger electron–phonon interaction as the CNTs undergo large tip rotations. The maximum temperature is nearly 600 K and such a temperature rise is not always at the middle region of the array.

4. Conclusion

A novel approach to obtain stabilised field emission current from a stacked CNT array is reported in this paper. A mesoscopic modelling technique is employed, which takes into account electro-mechanical forces in the CNTs, as well as transport of conduction electron coupled with electron–phonon induced heat generation from the CNT
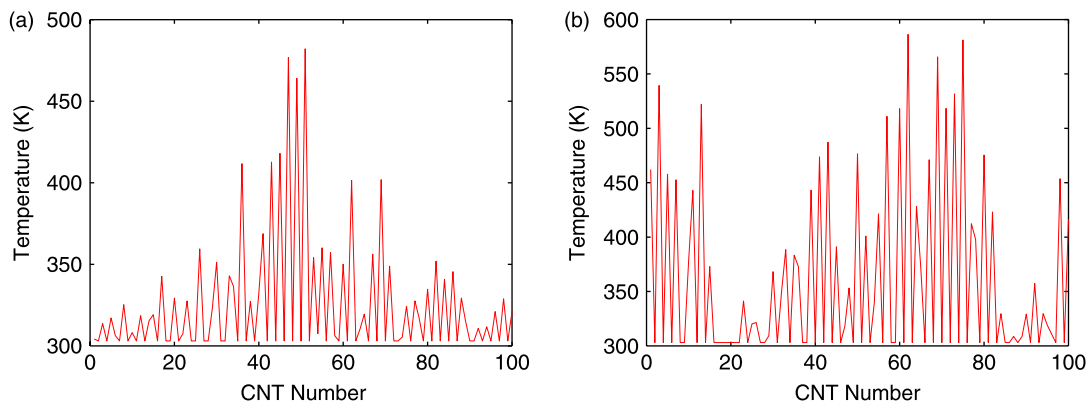
Figure 7.   Maximum temperature at the tip of each CNT for an array of 100 CNTs at $t = 50$ s of field emission for (a) pointed shape and (b) random height distribution.

tips. The reported analysis of pointed arrangements of the array shows that the current density distribution is greatly localised in the middle of the array, the scatter due to electrodynamic force field is minimised, and the temperature transients are much smaller compared to those in an array with random height distribution. Such arrays of CNTs, in pixel form, have important applications in biomedical X-ray devices and imaging. Based on this idea, a mechanically stable array of CNTs is likely to produce longer life, which requires further investigation.

References

[1] A.G. Rinzler, J.H. Hafner, P. Nikolaev, L. Lou, S.G. Kim, D. Tomanek, D. Colbert, and R.E. Smalley, *Unraveling nanotubes: field emission from an atomic wire*, Science 269 (1995), pp. 1550–1553.

[2] W.A. de Heer, A. Chatelain, and D. Ugrate, *A carbon nanotube field-emission electron source*, Science 270 (1995), pp. 1179–1180.

[3] L.A. Chernozatonskii, Y.V. Gulyaev, Z.Y. Kosakovskaya, N.I. Sinitsyn, G.V. Torgashov, Y.F. Zakharchenko, E.A. Fedorov, and V.P. Valchuk, *Electron field emission from nanofilament carbon films*, Chem. Phys. Lett. 233 (1995), pp. 63–68.

[4] J.M. Bonard, J.P. Salvetat, T. Stockli, L. Forro, and A. Chatelain, *Field emission from carbon nanotubes: perspectives for applications and clues to the emission mechanism*, Appl. Phys. A 69 (1999), pp. 245–254.

[5] Y. Saito and S. Uemura, *Field emission from carbon nanotubes and its application to electron sources*, Carbon 38 (2000), pp. 169–182.

[6] H. Sugie, M. Tanemure, V. Filip, K. Iwata, K. Takahashi, and F. Okuyama, *Carbon nanotubes as electron source in an X-ray tube*, Appl. Phys. Lett. 78 (2001), pp. 2578–2580.

[7] S.C. Lim, K. Lee, I.H. Lee, and Y.H. Lee, *Field emission and application of carbon nanotubes*, Nano 2(2) (2007), pp. 69–89.

[8] P.R. Schwoebel, *Field emission arrays for medical X-ray imaging*, Appl. Phys. Lett. 88 (2006), 113902.

[9] G.Z. Yue, Q. Qiu, B. Gao, Y. Cheng, J. Zhang, H. Shimoda, S. Chang, J.P. Lu, and O. Zhou, *Generation of continuous and pulsed diagnostic imaging X-ray radiation using a carbon-nanotube-based field-emission cathode*, Appl. Phys. Lett. 81(2) (2002), pp. 355–357.

[10] S. Wang, Z. Liu, S. Sultana, E. Schreiber, O. Zhou, and S. Chang, *A novel high resolution micro-radiotherapy system for small animal irradiation for cancer research*, Biofactors. 30(4) (2007), pp. 265–270.

[11] P. Yaghoobi and A. Nojeh, *Electron emission from carbon nanotubes*, Modern Phys. Lett. 21 (2007), pp. 1807–1830.

[12] R.V.N. Melnik and A. Povitsky, *A special issue on modelling coupled and transport phenomena in nanotechnology*, J. Comput. Theor. Nanosci. 3(4) (2006), doi: 10.1166/jctn.2006.001.

[13] R. Melnik, A. Povitsky, and D. Srivastava, *Mathematical and computational models for transport and coupled processes in micro- and nanotechnology*, J. Nanosci. Nanotechnol. 8(7) (2008), pp. 3626–3627.

[14] A. Buldum and J.P. Liu, *Electron field emission from carbon nanotubes: modeling and simulations*, Mol. Simul. 30 (2004), pp. 199–203.

[15] N. Sinha, D. Roy Mahapatra, J.T.W. Yeow, R.V.N. Melnik, and D.A. Jaffray, *Carbon nanotube thin film field emitting diode: understanding the system response based on multiphysics modelling*, J. Comput. Theor. Nanosci. 4 (2007), pp. 1–15.

[16] N. Sinha, D. Roy Mahapatra, Y. Sun, J.T.W. Yeow, R.V.N. Melnik, and D.A. Jaffray, *Electro-mechanical interactions in carbon nanotube based thin film field emitting diode*, Nanotechnology 19 (2008), 025701.

[17] D. Roy Mahapatra, N. Sinha, J.T.W. Yeow, and R. Melnik, *Field emission from strained carbon nanotube on cathode substrate*, Appl. Surf. Sci. 255(5) (2008), pp. 1959–1966.

[18] R. Melnik and R. Mahapatra, *Coupled effects in quantum dot nanostructures with nonlinear strain and bridging modelling scales*, Comput. Struct. 85(11–14) (2007), pp. 698–711.

[19] N. Sinha, D. Roy Mahapatra, R.V.N. Melnik, and J.T.W. Yeow, *Computational implementation of a new multiphysics model for field emission from CNT thin films*, M. Babuk et al., eds., *Lecture Notes in Computer Science*, ICCS 2008, Part II, LNCS 5102, 2008, pp. 197–206.

[20] N. Sinha, D. Roy Mahapatra, J.T.W. Yeow, and R.V.N. Melnik, *Multi-mode phonon controlled field emission from carbon nanotubes: device modeling and experiments*, IEEE Proceedings of 7th International Conference on Nanotechnology, 2007, pp. 961–964.

[21] M. Wang, Z.H. Li, X.F. Shang, X.Q. Wang, and Y.B. Zu, *Field enhancement array for carbon nanotube array*, J. Appl. Phys. 98 (2005), 014315.

[22] G. Chen, D.H. Shin, T. Iwasaki, H. Kawarada, and C.J. Lee, *Enhanced field emission properties of vertically aligned double-walled carbon nanotube arrays*, Nanotechnology 19 (2008), 415703.

[23] D. Roy Mahapatra, N. Sinha, S.V. Anand, R. Krishnan, N.V. Vikram, R.V.N. Melnik, and J.T.W. Yeow, *Design optimization of field emission from a stacked carbon nanotube array*, NSTI-Nanotech 2008, Vol. 1, 2008, pp. 55–58, ISBN 978-1-4200-8503-7.

[24] Y. Peng, Y. Hu, and H. Wang, *Fabrication of high-resolution multiwall carbon nanotube field emission cathodes at room temperature*, J. Vac. Sci. Technol. 25 (2007), pp. 106–108.

[25] G.Y. Slepyan, S.A. Maksimenko, A. Lakhtakia, O. Yevtushenko, and A.V. Gusakov, *Electrodynamics of carbon nanotubes: dynamic conductivity, impedance boundary conditions, and surface wave propagation*, Phys. Rev. B 60(24) (1999), pp. 17136–17149.

[26] L. Wei and Y.N. Wang, *Electromagnetic wave propagation in single-wall carbon nanotubes*, Phys. Lett. A 333 (2004), pp. 303–309.

[27] A. Svizhenko, M.P. Anantram, and T.R. Govindan, *Ballistic transport and electrostatics in metalic carbon nanotubes*, IEEE Trans Nanotech. 4 (2005), pp. 557–562.

[28] R.H. Fowler and L. Nordheim, *Electron emission in intense electric fields*, Proc. R. Soc. Lond. A 119 (1928), pp. 173–181.

[29] Z.P. Huang, Y. Tu, D.L. Carnahan, and Z.F. Ren, *Field emission of carbon nanotubes*, in *Encyclopedia of Nanoscience and Nanotechnology*, H.S. Nalwa ed.,Vol. 3, 2004, pp. 401–416.